

Article

A Novel Cycle Slips Detection and Repair Method with AR Model of BDS-3 Dual-Frequency Signal in Severe Multipath Environments

Yipeng Ning¹, Junye Cui¹, Wenshuo Zhao¹, Dashuai Chai^{1,*}, Yingjun Sun¹, Jianping Xing² and Shengli Wang³¹ College of Surveying and Geo-Informatics, Shandong Jianzhu University, Jinan 250101, China² College of Microelectronics, Shandong University, Jinan 250100, China³ College of Ocean Science and Engineering, Shandong University of Science and Technology, Qingdao 266590, China

* Correspondence: chaidashuai20@sdjzu.edu.cn

Abstract: High-level applications of geo-processing services generally lack accurate temporal and spatial information. BDS-3 provides high precision temporal and spatial reference for geoprocessing services, but their signal is prone to cycle slips in a severe multipath environment. Aiming at the problem of the reliable detection and repair of cycle slips in BDS-3 (B1c + B2a) dual-frequency positioning in a severe multipath environment, an AR (autoregressive) model-assisted MW + GF BDS dual-frequency combined detection method (AMG method) is proposed in this research. A sliding-window autoregressive prediction strategy is introduced to correct the pseudorange observations interfered by a multipath, then an AR + MW + GF cycle slips detection model is constructed, and a cycle slips statistical completeness test index is established to verify the effectiveness of the algorithm. Six groups of cycle slips are artificially added into the different constellations and dual-frequency point phase observations of BDS-3 (B1c and B2a) in a multipath environment to demonstrate the cycle slips' detection performance. The experimental results show that the traditional MW + GF method fails, but the proposed AMG method still maintains accurate cycle slip detection and repair capabilities. The detection success rate and repair success rate obtained by using the new method are significantly improved by 63.4%, and the cycle slips' false detection rate and missed detection rate are reduced by 64.5% and 42.0%, respectively, even in harsh environments.

Keywords: geoprocessing services; BDS-3; cycle slips; AR model; GF combination; MW combination



Citation: Ning, Y.; Cui, J.; Zhao, W.; Chai, D.; Sun, Y.; Xing, J.; Wang, S. A Novel Cycle Slips Detection and Repair Method with AR Model of BDS-3 Dual-Frequency Signal in Severe Multipath Environments. *Appl. Sci.* **2023**, *13*, 27. <https://doi.org/10.3390/app13010027>

Academic Editor: Jianbo Gao

Received: 15 November 2022

Revised: 13 December 2022

Accepted: 18 December 2022

Published: 20 December 2022



Copyright: © 2022 by the authors. Licensee MDPI, Basel, Switzerland. This article is an open access article distributed under the terms and conditions of the Creative Commons Attribution (CC BY) license (<https://creativecommons.org/licenses/by/4.0/>).

1. Introduction

In recent years, the rapid development of the Internet and big data has promoted the rapid development of the field of geographic information science, and geographical users' demands for geoprocessing services have become more personalized and diversified. However, the geoprocessing service which lack temporal and spatial information cannot meet the higher application requirements of users gradually [1–4]. The BDS system and other global navigation satellite systems can provide universal and unified high-precision positioning, navigation and timing (PNT) services for geoprocessing services globally [5]. In order to achieve compatibility and interoperability with GPS and Galileo satellite navigation systems, the BDS-3 system broadcasts new frequency points B1c (1575.420MHz) and B2a (1176.450MHz) system signals on the launched MEO and IGSO satellites to provide global services [6,7]. The new frequency points can increase the number of observable satellites and the continuity of the data in the observation period, thus improving the reliability of high-precision positioning [8]. However, in the harsh environment, influenced by the urban canyon et al, the signal multipath is easy to occur, which leads to frequent cycle slips, and the carrier phase measurement is difficult to reach the centimeter-level accuracy, even causing a signal interruption and being unable to secure the positioning [9]. Therefore,

when the BDS high-precision positioning is performed, the cycle slips in the original observation value must be detected and repaired.

For the dual-frequency cycle slips detection method, the high-order difference method between epochs [10], the Doppler integration method [11], and the TurboEdit method, they utilize Melbourne–Wübbena (MW) [12] and geometry-free (GF) combinations [11–15]. The TurboEdit algorithm improves the reliability of the detection of cycle slips by combining the MW and GF method, becoming the most commonly used method for dual-frequency cycle slips processing [16]. However, dual-frequency signals have longer wavelengths, but are also subject to more multipath effects [17]. Especially for the MW combination, false detection occurs frequently in a severe multipath environment and it is difficult to detect 1–2 cycle slips, and sometimes the MW combination even fails.

In order to reduce the influence of pseudorange errors and improve the cycle slips detection capability in a severe multipath environment, many scholars have put forward different ideas. The first category is to improve the TurboEdit algorithm, for instance, Miao (2011) improved the TurboEdit method [18] by introducing a satellite altitude angle weighting factor into the MW combination, but this method does not change the issue that the MW combination noise is too large to detect the small cycle slips of the GNSS measurements. Xu (2020) proposed an improved TurboEdit cycle slip detection and repair method, which uses the ultra-wide lane combination with a difference between epochs to estimate the changes in the smartphone position and clock skew and identifies the cycle slip by checking the maximum normalized residual [19], but it is not satisfactory in complex environments. Dong (2021) used the method of dividing the cycle slips' arc segment based on the multipath RMS size to repair the multipath value hopping to 0m, and then used the TurboEdit method for a joint detection, which improved the cycle slips' detection efficiency and further improved the dual-frequency positioning accuracy [20]. The second category is to weaken the pseudorange errors, e.g., Cai (2013) combined the forward and backward moving window (FBMWA) algorithm with the second-order time-difference phase ionospheric residual (STPIR) algorithm to reduce the influence of large pseudorange errors to improve the cycle slips' detection accuracy [21], but its moving window cannot contain the cycle slips data, which is difficult to satisfy in real life. Li (2021) proposed a BDS dual-frequency signal cycle slips detection and repair method (BDCSR) to construct a discriminant function to repair cycle slips, which overcomes the interference of large pseudorange errors, and not only eliminates the influence of pseudorange errors, but also has a good recognition misjudgment capability [12]. Shi (2021) adopts the phase-Doppler combination and the geometry-free combination to detect cycle slips and uses the simple rounding method with the dual-frequency least-square ambiguity decorrelation adjustment (LAMBDA) method to repair the cycle slips. This method reduces the influence of the multipath effect, but it requires a high sampling rate and a stable ionospheric environment to be effective [22]. Li (2019) proposed a novel method relying on the satellite orbit and smoothed pseudorange. This method solves the error of the cycle slips' detection results caused by the gross error on the pseudorange, but is only suitable for a single GNSS system due to the limitation of computation [23]. Gao (2018) used BDS tri-frequency data and considered the multipath effect when setting the threshold in a fixed single epoch ambiguity. Although the random noise can be reduced by filtering and smoothing, the non-random multipath errors cannot be effectively suppressed in a short time [24]. In addition to these above methods, many scholars also use other sensor observations to improve the performance of the detection of cycle slips, e.g., Ning (2016) used inertial information to assist the Beidou tri-frequency to improve the success rate of detecting cycle slips and repair the rate in the case of serious multipath errors. This method overcomes the shortage of the accuracy of pseudorange observations, but its INS prediction error increases with time [25]. Kim (2020) constructed a time difference carrier phase (TDCP)/INS system by using multiple constellations, which ignored system time differences, and judged whether the TDCP system performed abnormally for the cycle slips' detection and repair through

the INS prediction error range [26]. Such INS-aided method surely shows quite a good detection ability, however, they require additional sensors.

The above research either improved the MW + GF combination method or adopted different auxiliary methods to weaken the influence of pseudorange multipath effects dramatically, but in a severe multipath environment, even if a high sampling frequency is employed, the multipath effect cannot be completely eliminated in the case of an epoch difference, especially if the pseudorange multipath residual seriously affects the cycle slips' detection capability of the MW combination. At present, the reliable detection and repair of BDS3 (B1c + B2a) double-frequency cycle slips in complex environments is still worthy of further study. Therefore, for the carrier phase cycle slips detection and repair on BDS-3 B1c (hereinafter referred to as P1 and L1) and B2a (hereinafter referred to as P5 and L5) frequencies under a severe multipath, we propose an AR model-assisted MW + GF BDS dual-frequency combined detection method (AMG method). In this method, the satellite-to-ground distance observation data unaffected by the multipath were used as the training volume, an AR model was built based on the sliding-window method to predict the reliable satellite-to-ground distance observation data in the multipath environment, and then the cycle slips detection model of the AR combined with MW + GF method was derived. The completeness monitoring index was introduced to analyze the detection performance, and finally the cycle slips were repaired by the MW combination.

The rest of this paper is structured as follows. Section 2 introduces the mathematical model of the cycle slips' detection and repair. Sections 3 and 4 introduces the experimental design and results.

2. Methods

In this section, a novel cycle slips detection method is introduced to solve the anomaly problem of double frequency BDS-3 observations in a severe multipath environment. Firstly, the conventional cycle slips detection model of a geometry-free phase combination and Melbourne–Wübbena combination is described in detail. Secondly, an AR model was constructed with a sliding-window method by selecting the pure pseudorange observations as the training quantity. By this means, the MW combination observation equation is reconstructed by using the predicted dual-frequency pseudorange observation values, and the AMG combined cycle slips detection model and estimation is rigorously derived. Finally, the completeness monitoring index is introduced to analyze the performance of the proposed method.

2.1. Cycle Slips Detection Model with Geometry-Free Phase Combination

In a GF combination, the ionosphere residuals of the dual-frequency carrier phase observations are utilized to detect cycle slips, and therefore the effects of the geometric distance are eliminated. For the purpose of this study, the GF observation is expressed as [27]:

$$L_{GF} = L_1 - L_5 = \lambda_1 N_1 - \lambda_5 N_5 + \frac{f_1^2 - f_5^2}{f_5^2} ion \quad (1)$$

where the symbol c denotes the speed of light, L_1, L_5 are the raw carrier phase observations of B1c and B2a, respectively, and the carrier phase frequencies are f_1 (1575.420 MHz), f_5 (1176.450 MHz), $\lambda_1 = (c/f_1)$, and $\lambda_5 = (c/f_5)$. The geometric distance between the stations and satellites have been eliminated by Equation (1), and also the satellite clock error and the receiver clock error. If we take the adjacent epoch difference of Equation (1), then the decision quantity of the GF combination can be constructed for the cycle slips' detection:

$$\Delta N_{GF} = L_{GF}(t+1) - L_{GF}(t) \quad (2)$$

In this formula, ΔN_{GF} represents a cycle-slip detection measurement without a geometry model.

According to the law of error propagation, we obtain the standard deviation of the GF combined cycle slips' detection:

$$\sigma_{\Delta N_{GF}} = \sqrt{2} \cdot \sqrt{(\sigma_{\varphi})^2 + \left(\frac{f_1}{f_5}\sigma_{\varphi}\right)^2} \tag{3}$$

where the standard deviation of the cycle slips' detection for the GF model is $\sigma_{\Delta N_{GF}} = 0.023$ cycles. The carrier phase precision is $\sigma_{\varphi} = 0.01$ cycles [28]. In this paper, 3 times the standard deviation is taken as the threshold to test the occurrence of cycle slips; when the cycle slip detection value of the B1c and B2a carrier phase observation is greater than 0.07 cycles, it can be judged that the phase observation has cycle slips.

2.2. Cycle Slips Detection Model of Melbourne–Wübbena Combination

The MW combination is a linear model obtained by subtracting the narrow-lane combination of pseudorange from the wide-lane combination of the carrier phase, which can eliminate the influence of the geometric distance, atmosphere, and clock difference on the detection of cycle slips. The MW combination can be expressed as [29]:

$$L_{MW} = \frac{1}{f_1 - f_5} (f_1 L_1 - f_5 L_5) - \frac{1}{f_1 + f_5} (f_1 P_1 + f_5 P_5) \tag{4}$$

where L_{MW} are the MW combination observations and P_1, P_5 are the pseudorange observations of B1c and B2a, respectively. The rest of the symbols are the same as formula (1). The wide-lane wavelength is $\lambda_{MW} = c / (f_1 - f_5)$. L_{MW} can eliminate the influence of factors such as the inter-station distance, atmospheric delay error, satellite clock error, etc., and simply retain the influence caused by the multipath effects and observation noise, which can be weakened or eliminated by making differences between epochs. Its expression is:

$$\Delta N_{MW} = \frac{L_{MW}(t+1)}{\lambda_{MW}} - \frac{L_{MW}(t)}{\lambda_{MW}} \tag{5}$$

where ΔN_{MW} is the detection value of the cycle slips of the MW combination after the difference between epochs, that is, the cycle slips' estimation.

Equation (4) can be simplified as $L_{MW} = L_{WL} - P_{NL}$, where L_{WL} is the wide-lane phase combination (WL) and P_{NL} is the narrow-lane pseudorange combination (NL),

Therefore, L_{WL} , the carrier phase wide-lane phase combination of BDS B1c and B2a, can be expressed as:

$$L_{WL} = \alpha_{WL} L_1 + \beta_{WL} L_5 \tag{6}$$

Its combination coefficient can be described as: $\alpha_{WL} = f_1 / (f_1 - f_5)$ and $\beta_{WL} = -f_5 / (f_1 - f_5)$ [30].

Similarly, the narrow-lane combination P_{NL} code combination is given as:

$$P_{NL} = \alpha_{NL} P_1 + \beta_{NL} P_5 \tag{7}$$

The combination coefficient in Equation (7) is: $\alpha_{NL} = f_1 / (f_1 + f_5)$ and $\beta_{NL} = f_5 / (f_1 + f_5)$.

It is assumed that the carrier phase observations and the pseudorange observations are independent of each other and have the same accuracy. Then, the standard deviation of the MW combination cycle slips' estimation can be approximately expressed as:

$$\sigma_{\Delta N_{MW}} = \sqrt{(\alpha_{WL}\sigma_{\varphi})^2 + (\beta_{WL}\sigma_{\varphi})^2 + \left(\frac{\alpha_{NL}\sigma_P}{\lambda_{mw}}\right)^2 + \left(\frac{\beta_{NL}\sigma_P}{\lambda_{mw}}\right)^2} \tag{8}$$

where σ_{φ} is the precision of the carrier phase observations, which is 0.01 cycles in this paper, and σ_P is the precision of the pseudorange observations, which is 0.3 m [31] in this paper.

Under normal circumstances, the influence of the multipath on the pseudorange observations is much greater than that of the carrier phase observations. If the GF combination does not adopt the pseudorange observations, it will not alarm when the multipath conditions occur. When the multipath effect is quite serious, the multipath residual between epochs should be regarded as white noise, then the standard deviation equation of the MW combination cycle slips' estimation should be rewritten as:

$$\sigma_{\Delta N_{MW,M}} = \sqrt{(\alpha_{WL}\sigma_\varphi)^2 + (\beta_{WL}\sigma_\varphi)^2 + \left(\frac{\alpha_{NL}\sigma_P}{\lambda_{mw}}\right)^2 + \left(\frac{\beta_{NL}\sigma_P}{\lambda_{mw}}\right)^2 + \left(\frac{M_1^2 + M_2^2}{\lambda_{mw}^2}\right)} \quad (9)$$

2.3. AMG Combined Cycle Slip Detection Model

Most cycle slips processing methods are based on the linear combinations of pseudorange and the phase observation. The severe multipath in complex environments seriously affects the pseudorange accuracy, resulting in significant deviations in the MW combination cycle slips' estimation. In order to effectively utilize the pseudorange phase to detect and repair cycle slips, an AMG combined cycle slips detection method is proposed in this paper. First, an autoregressive (AR) model prediction method was used to predict pseudorange observations in a multipath environment. Then, an MW + GF combined cycle slips detection model was used to correct the cycle slips' estimation with the predicted pseudorange observations. Compared with the traditional MW method, the AMG method can effectively solve the cycle slips' detection problem in severe multipath conditions, and false detection rarely occurs.

An AR model is a kind of widely used time series model. The prediction result at time t can be represented by a linear combination of the observations at time y before or after it, and its expression is as follows [32]:

$$z_t = \sum_{i=1}^p \theta_i z_{t-i} + \varepsilon_t \quad (10)$$

where z_t represents the predicted value, θ_i represents the autoregressive coefficient, y represents the model order, and ε_t represents the system noise.

The y -order AR model of the pseudorange P is established based on the sequential characteristic. In order to improve the performance of cycle slips' detection in a multipath environment, more accurate pseudorange observations are required; that is, the difference between the actual pseudorange observations and the predicted values is required to be as small as possible. Therefore, a sliding window is constructed based on the pseudorange observations without multipath contamination to predict the pseudorange observations in the multipath environment:

$$\begin{aligned} p[1] &= a_1 p[0] + \varepsilon[n] \\ p[2] &= a_1 p[1] + a_2 p[0] + \varepsilon[n] \\ &\vdots \\ p[n] &= a_1 p[n-1] + a_2 p[n-2] + \dots + a_y p[n-y] + \varepsilon[n] \end{aligned} \quad (11)$$

Assuming that the different pseudoranges are of an equal accuracy, the accuracy σ_z predicted by the AR model can be inferred based on the error propagation law [33]:

$$\sigma_z = \sqrt{a_1^2 + a_2^2 \dots a_n^2} \cdot \sigma_p^2 \quad (12)$$

The order of the AR model has a great influence on the accuracy of its prediction. So the least squares and the final prediction error (FPE) criterion ($FPE(n) = \frac{N+n}{N-n} \sigma_a^2$), the information (AIC) criterion ($FPE(n) = \frac{N+n}{N-n} \sigma_a^2$), and the BIC criterion ($FPE(n) = \frac{N+n}{N-n} \sigma_a^2$) are used to jointly test the applicability in this paper. In order to save space, the results of

the joint test are directly given, that is, the optimal model is taken when the model order is $y = 3$ by the joint test.

Based on Equation (12), the MW combined observation equation assisted by the predicted value of the AR model can be obtained:

$$L'_{MW} = \frac{1}{f_1 - f_5} (f_1 L_1 - f_5 L_5) - \frac{1}{f_1 + f_5} (f_1 z_{t(P_1)} + f_5 z_{t(P_5)}) \tag{13}$$

By differencing the combined equations of two adjacent epochs, we can obtain:

$$\Delta N'_{MW} = \frac{L_{MW'}(t+1)}{\lambda_{MW}} - \frac{L_{MW'}(t)}{\lambda_{MW}} \tag{14}$$

Therefore, the standard deviation of the AR-assisted MW combination cycle slips' estimation is:

$$\sigma_{\Delta N_{MW}} = \sqrt{(\alpha_{WL}\sigma_\varphi)^2 + (\beta_{WL}\sigma_\varphi)^2 + \left(\frac{\alpha_{NL}\sigma_{zP}}{\lambda_{mw}}\right)^2 + \left(\frac{\beta_{NL}\sigma_{zP}}{\lambda_{mw}}\right)^2} \tag{15}$$

where σ_z is the prediction accuracy of the AR model. Compared with the traditional MW combination observations, the MW observation values assisted by the AR model are not affected by the pseudorange multipath and pseudorange noise, but only by the prediction accuracy. In a severe multipath environment, the AMG method has a more accurate detection advantage than the traditional combination.

2.4. Cycle Slips Completeness Test

The mathematical rationale for the detection and repair of cycle slips is based on statistical hypothesis testing. Cycle slip detection and repair consists of two distinct tasks. The first is to identify whether a cycle slip occurs in the observed value, and the second is to calculate the cycle slips' value and repair the cycle slips [34].

A system modeling method based on hypothesis testing is used to construct cycle slips test statistics. If there are no cycle slips, the probability density function follows a Gaussian distribution with a mean of 0. However, if there are cycle slips in the observed value, the probability density function follows a Gaussian distribution with a mean of b , and the standard deviation is both σ , which is expressed by:

$$H_1 : DV \sim N(b, \sigma) \tag{16}$$

$$H_0 : DV \sim N(0, \sigma) \tag{17}$$

where b is the size of the cycle slips.

Then, the false alarm rate and the missed alarm rate of the cycle slips' detection can be established as [35]:

$$P_F = P(|DV| \geq T_D | H_0) = \text{erfc}\left(\frac{T_D}{\sqrt{2}\sigma}\right) \tag{18}$$

where T_D is the set cycle slips' detection threshold.

Corresponding to the false alarm rate, the missed alarm rate represents the probability that the cycle slips does exist, but the threshold is not exceeded. The missed alarm rate can be expressed as [35]:

$$P_M = P(|DV| < T_D | H_1) = \text{erfc}\left(\frac{b - T_D}{\sqrt{2}\sigma}\right) - \text{erfc}\left(\frac{b + T_D}{\sqrt{2}\sigma}\right) \tag{19}$$

where $erfc(x) = \frac{2}{\sqrt{\pi}} \int_x^\infty e^{-t^2} dt$, the detection threshold is $T_D = m\sigma_{\Delta N_{MW}}$. The maximum missed detection rate is obtained when $b = 1$ [35]. When $m = 3$ (99.73% confidence level), an optimal combination is obtained [35].

Due to the multipath effect, the accuracy of the pseudorange is seriously affected by the traditional method, which leads to the failure of the rounding repair. When the model detects cycle slips, the approximate number of cycle slips ΔN_{MW} is repaired by (similarly to ΔN_{GF}):

$$N_1 = \text{round}(\Delta N_{MW}) \tag{20}$$

where round means to find the integer value closest to ΔN_{MW} .

The success rate of the cycle slips' repair can be expressed as [36,37]

$$P_0 = 1 - \sum_{i=1}^{\infty} [erfc(\frac{i - |\Delta N_1 - \text{round}(\Delta N_1)|}{\sqrt{2}\sigma}) - erfc(\frac{i + |\Delta N_1 - \text{round}(\Delta N_1)|}{\sqrt{2}\sigma})] \tag{21}$$

Given a confidence level α , if P_0 is greater than α , the cycle slips' repair can be considered successful. The flowchart of the proposed algorithm is shown in Figure 1.

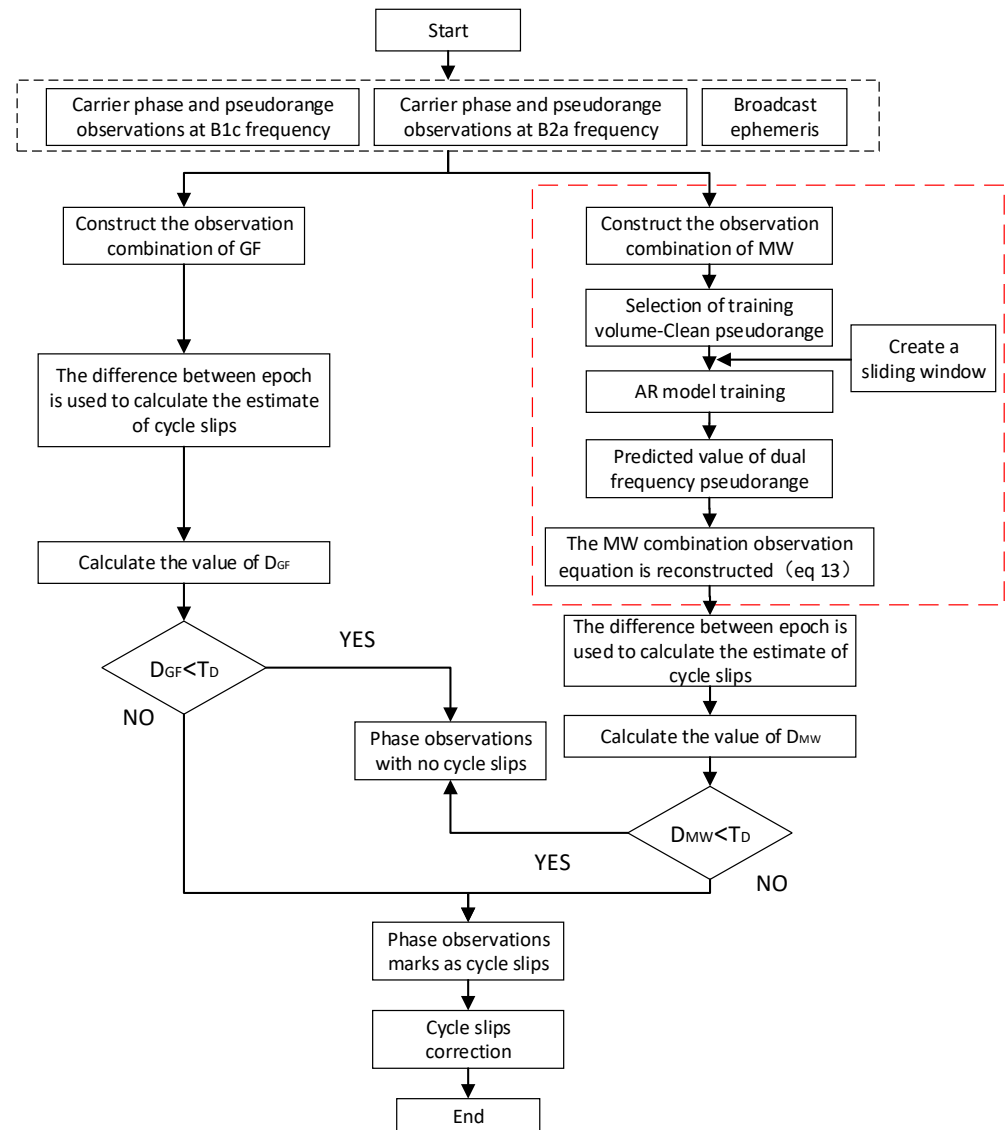


Figure 1. Flow chart of AMG cycle slip detection and repair method.

3. Experiment and Analysis

In this section, the AMG cycle slips detection method is evaluated through a field test by collecting BDS observations in the severe multipath environment and weak multipath environment. First, the experimental design is described in detail. Second, the influence of the multipath environment on the cycle slips' detection and cycle slips' completeness is tested and analyzed. In the end, several different groups of cycle slips are added artificially to validate our points.

3.1. Field Test Design

In order to evaluate the accuracy and reliability of the proposed AMG combined cycle slips detection and repair method, two experiments are designed. In Experiment 1, the BDS observation data under a severe multipath environment were collected from Yingxue Lake on the Shandong Jianzhu University (SDJZU) campus to evaluate the influence of the multipath on the cycle slips' detection. In Experiment 2, the BDS observation data in a weak multipath environment was collected from a roof of SDJZU to verify the feasibility of the proposed algorithm. The experimental scene is shown in Figure 2, and in both experiments, the GNSS base station was located on the top of another building. The data acquisition time was DOY96 and DOY100 of 2022, and the sampling interval was 1 s. The GNSS equipment was the chcnv i70II receiver, which could receive BDS3 dual-frequency signals. The sampling time of the two experiments was 2000 and 2500 epochs, respectively. In order to test the performance of the cycle slips' detection and repair in a multipath environment, pseudorange and carrier phase observations of the B1c and B2a frequency of the C38 satellite (MEO satellite) and C40 satellite (IGSO satellite) in Experiment 2 were selected, and the multipath effect was simulated in 500–2500 epoch of the observed data, and the cycle slips of 1–8 cycles were artificially added. The experimental data before and after adding simulated cycle slips were processed and analyzed with the method proposed in this paper.



(a)



(b)

Figure 2. Experimental area and scene: (a) severe multipath environment; (b) weak multipath environment.

3.2. Analysis of Influence of Multipath Environment on Cycle Slips Detection

The dual-frequency data of 2000 epoch static observations of PRN38 and PRN40 satellites for BDS-3 MEO and IGSO constellations collected in Experiment 1 are analyzed. The method in reference [38] was used to calculate the multipath effect and its variation between epochs, as shown in Figures 3 and 4.

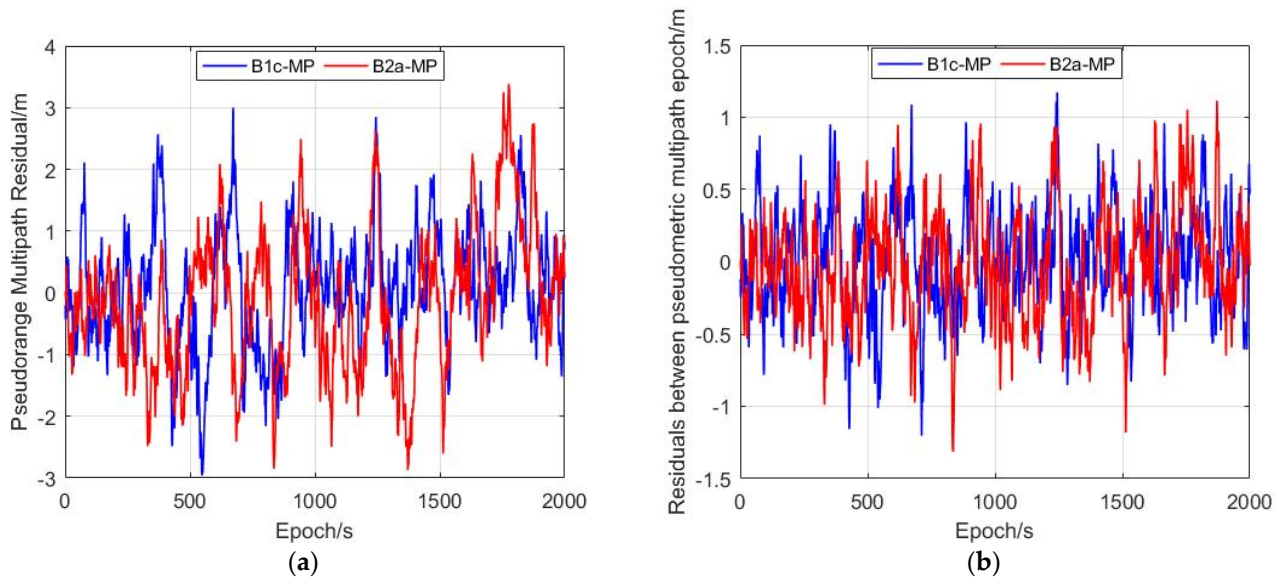


Figure 3. The multipath effect of PRN38 satellite: (a) multipath effect situation; (b) residuals between multipath epochs.

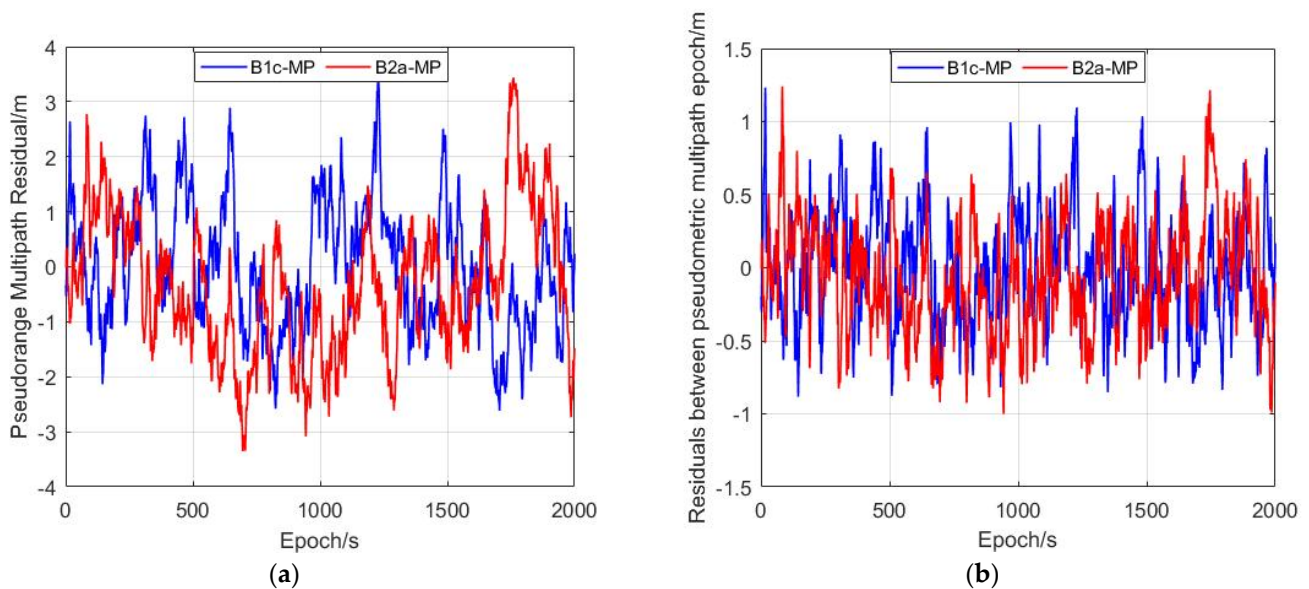


Figure 4. The multipath effect of PRN40 satellite: (a) multipath effect situation; (b) residuals between multipath epochs.

According to Figures 3 and 4, in the severe multipath environment, the pseudorange multipath effect of the two frequency points is at the meter level. The change amplitude of the multipath effect is similar for the B1c and B2a frequency, and the maximum values of the multipath effects between the B1c and B2a frequency epoch were C38 (1.202 m and 1.314 m) and C40 (1.234 m and 1.242 m), respectively. According to the above multipath variation, a similar multipath effect is simulated in 500 to 2500 epoch of the Experiment

2 data. The cycle slips estimation of the MW combination after simulating the multipath effect is shown in Figure 5.

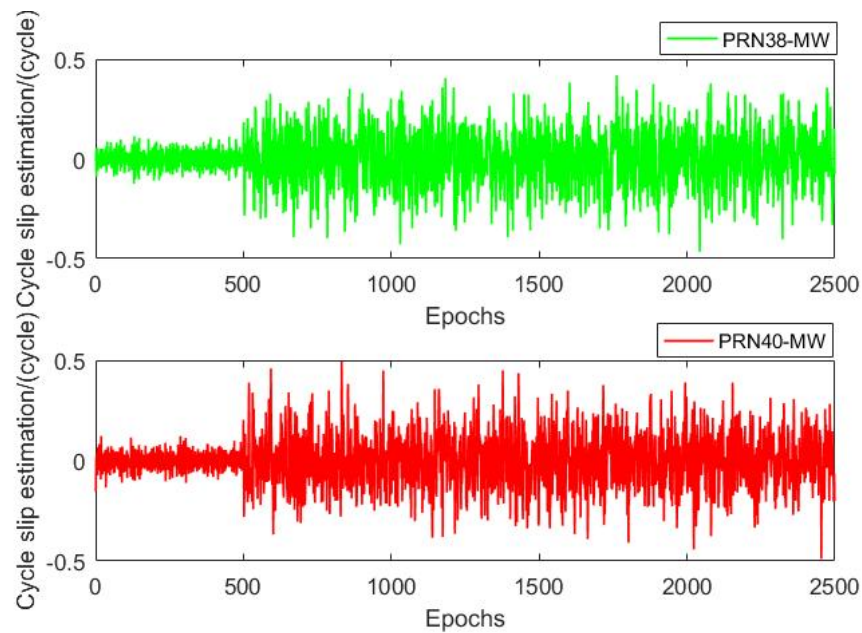


Figure 5. Simulated cycle slips detection of multipath phenomenon.

Based on the above amount of variation, the cycle slips’ estimation of the two frequency points can be set to $M_1 = 1$ m and $M_2 = 1$ m, respectively. As shown in Table 1, when the system is seriously affected by the pseudorange multipath, the false detection rate reaches 64% and the missed detection rate reaches 42%. This is because the multipath effect leads to abnormal fluctuations in the pseudorange in the MW combination, the overall narrow-lane combination becomes smaller, and the cycle slips’ estimation becomes larger, so the pseudorange multipath effect is misdetected as cycle slips. Especially for the short wavelength of the dual-frequency signal combination, the false detection and missing detection are even more serious.

Table 1. False detection rate and missed detection rate statistics.

Different Environments	Detection Combinations	PRN	PF	PM	$\sigma_{\Delta N_{ij,AR}}/Cycles$
No multipath environment	MW	C38	0.27%	0.01%	0.2895
		C40	0.27%	0.01%	0.2895
Severe multipath environment	MW	C38	64.83%	42.04%	1.9042
		C40	64.83%	42.04%	1.9042
	AR + MW	C38	0.29%	0.01%	0.2919
		C40	0.29%	0.01%	0.2920

Figures 6 and 7 give the cycle slips estimations of the PRN38 and PRN40 satellite observations under the multipath effect using the dual-frequency MW and GF detection models. The MW combination (at 500~2500 epochs) shows a trend term that is clearly affected by the multipath, with the cycle slips’ estimations of multiple epochs exceeding 0.4 cycles. The false detection rate is 64%, which is very serious; while on the contrary, the GF combination is not affected by the pseudorange multipath influence and still maintains a good detection capability. The results indicate that the traditional MW detection model fails in a severe multipath environment.

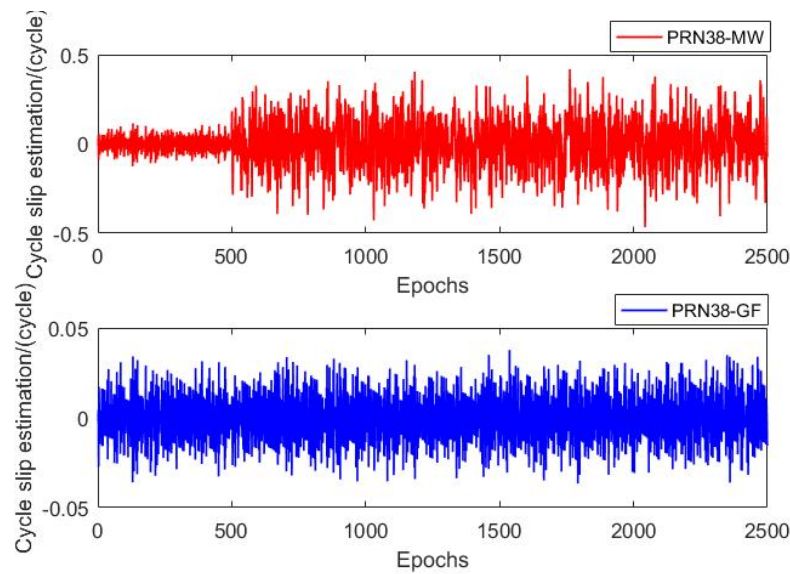


Figure 6. PRN38 cycle slips estimated value under multipath effects.

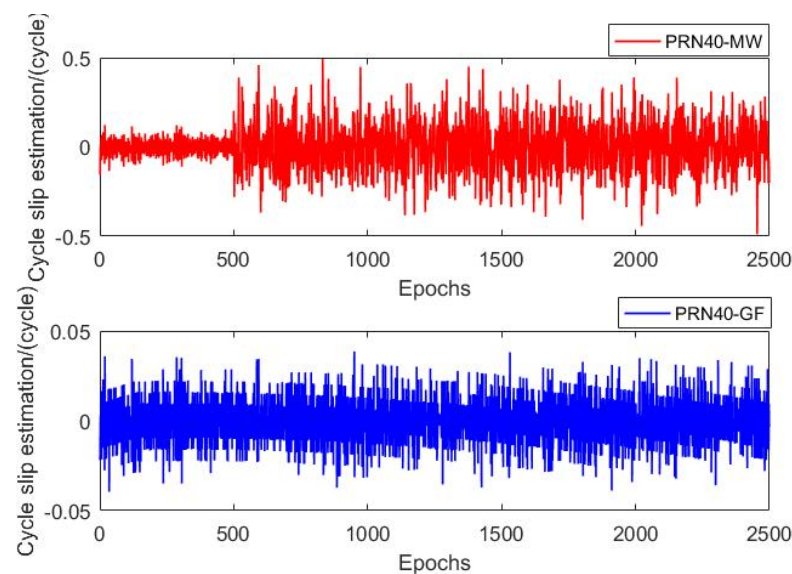


Figure 7. PRN40 cycle slips estimated value under multipath effects.

3.3. Analysis of the Results of the AMG Combined Cycle Slip Completeness Detection

The cycle slips' detection and repair of the MW combination method assisted by an AR model are carried out on the same data of Experiment 2 in Section 3.1, and the effectiveness and reliability of this method are verified by comparison. In order to achieve a false detection rate of 5%, that is, $\sigma_{\Delta N_{MW,M}}$ should be less than 0.443 cycles, and the pseudorange multipath errors of the two frequency points should be less than 0.2 m.

Firstly, a 500 epochs sliding-window with time series characteristics is constructed by using pseudorange data not contaminated by the multipath, and the AR model is used to predict pseudorange observations in a severe multipath environment according to the time-domain characteristics of the sliding-window. The predicted residuals are shown in Figure 8. The experimental results show that the predicted mean value of the pseudorange observations is 0.028 m, and the proportion of the predicted residuals less than 0.1 m is more than 96%.

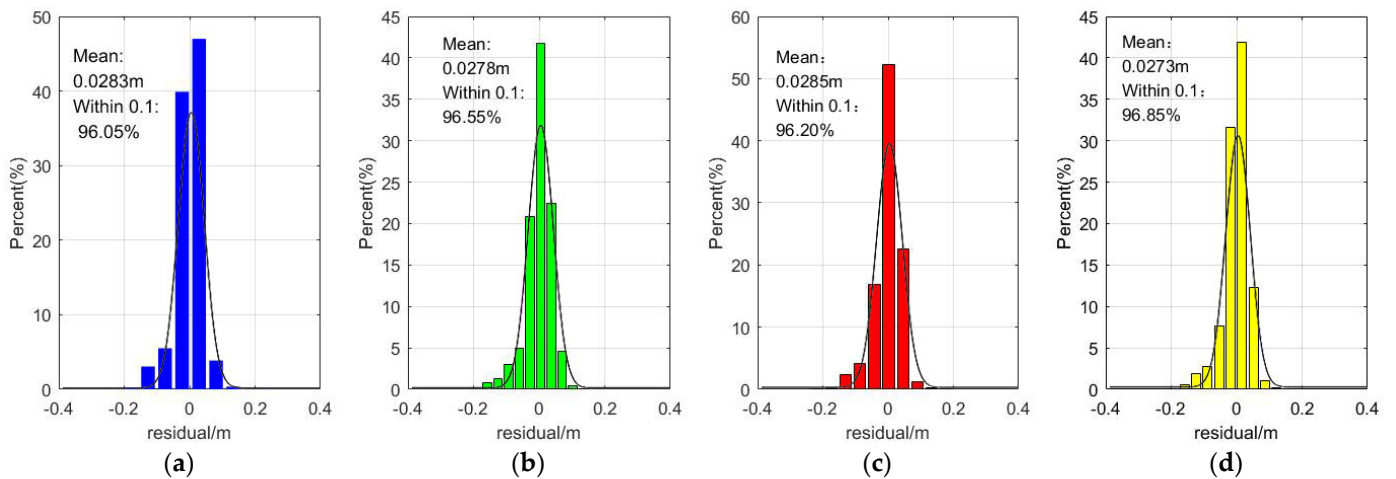


Figure 8. Pseudorange residuals predicted by AR model: (a) C38 P1 predicted residual; (b) C38 P5 predicted residual; (c) C40 P1 predicted residual; (d) C40 P5 predicted residual.

The AR model-assisted MW combined cycle slips’ detection estimations are shown in Figure 9. Comparing Figure 4, the pseudorange multipath effect of the method used in this paper is significantly suppressed, and the cycle slips’ estimations are all less than 0.2 cycles. As shown in Table 1, the detection estimation assisted by the AR model is 0.2919 cycles, which is close to 0.2895 cycles in the case of no cycle slips and significantly lower than 1.9042 cycles in the multipath environment, indicating that the cycle slip estimation is more accurate. At the same time, the false detection rate and miss detection rate of this method are less than 1%, so the AR+MW combination still maintains a powerful detection ability in a severe multipath environment.

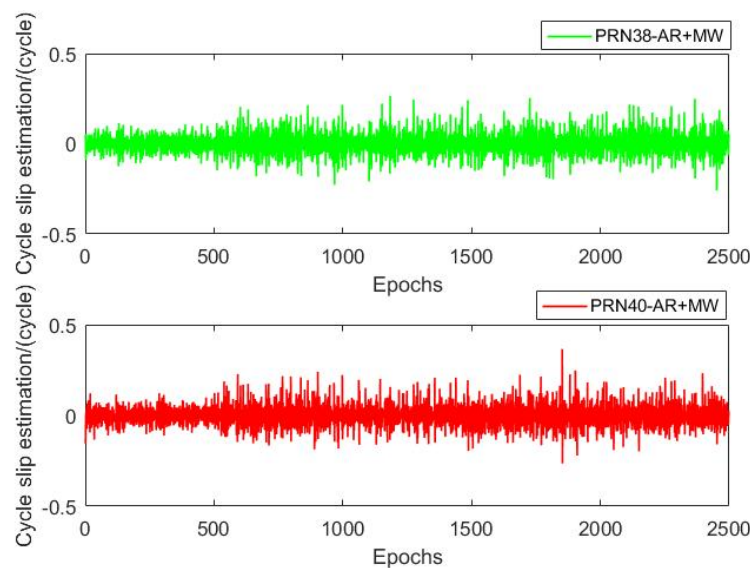


Figure 9. PRN38 and PRN40 cycle slips estimated value based on AR model assistance.

3.4. Analysis of AMG Combined Cycle Slip Detection Results

In order to test the detection capability of the AMG combination for cycle slips in a severe multipath environment, both frequencies of the MEO C38 and IGSO C40 satellites of different constellations were added with 1–8 cycles of scattered small cycle slips in a severe multipath environment. The added cycle slips combinations are shown in Table 2.

Table 2. Size and position of simulated cycle slips.

Epoch	700	900	1300	1700	2000	2300
cycle slips	1	2	8	1	−1	5
	1	4	6	−2	1	3

Figure 10 shows the cycle slips’ detection result of the traditional MW + GF combination. Figure 11 shows the cycle slips detection result of the AMG model, and the comparison of the completeness detection is shown in Figure 12. The repair results are shown in Table 3.

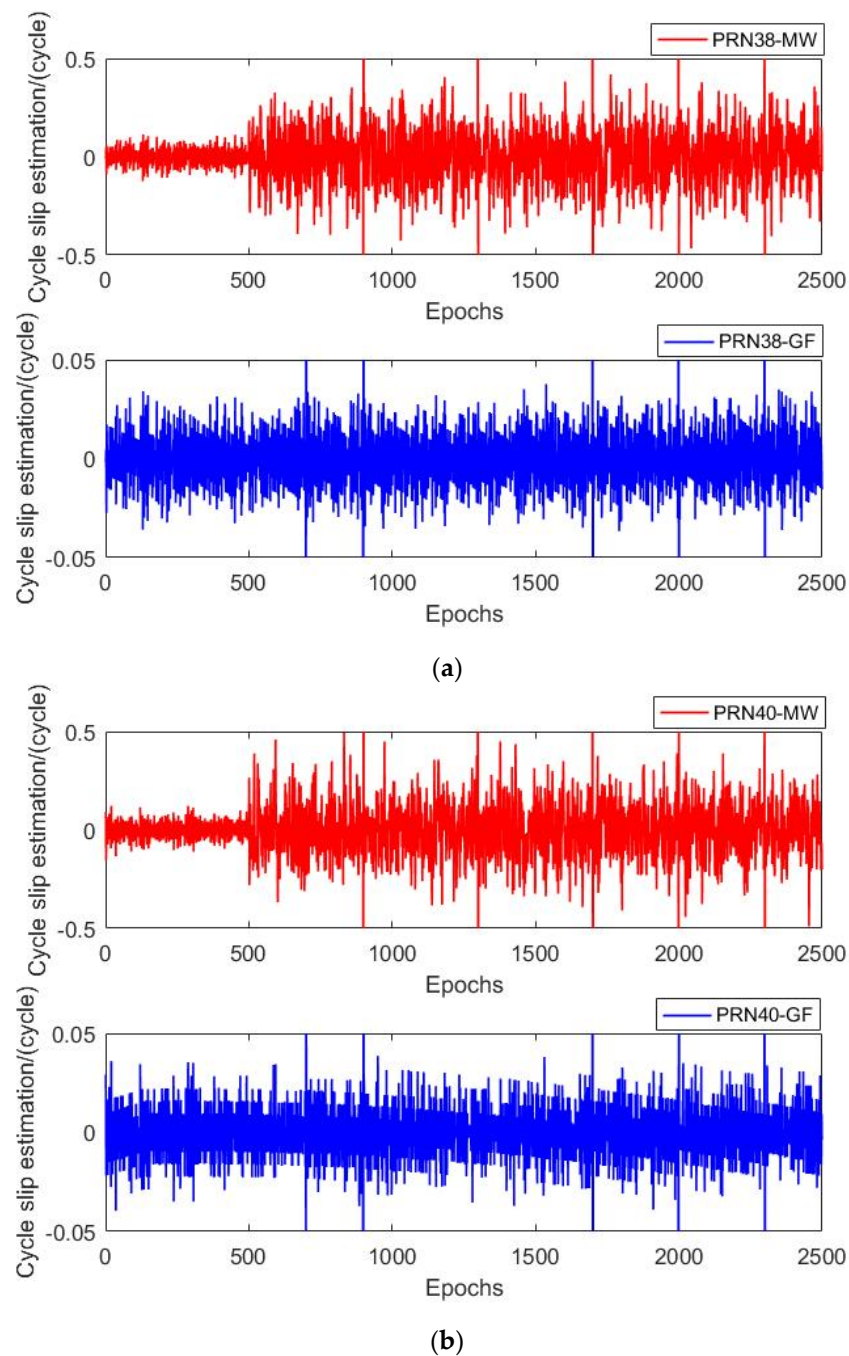


Figure 10. Cycle slip detection results of PRN38 and PRN40 MW + GF combinations in a multipath environment: (a) PRN38 cycle slips estimated value; (b) PRN40 cycle slips estimated value.

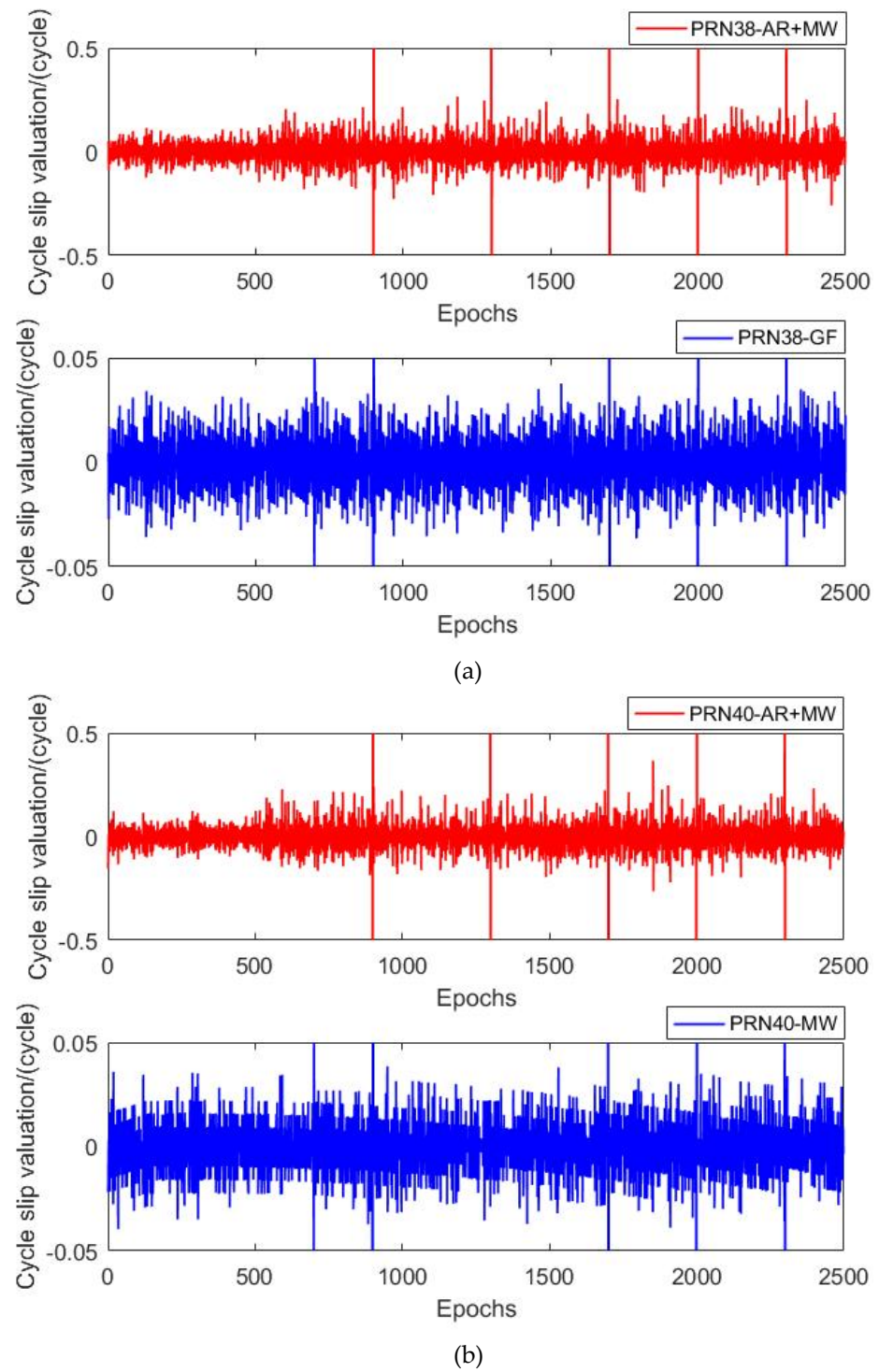


Figure 11. Cycle slips detection results of PRN38, PRN40 AMG combinations in a multipath environment: (a) PRN38 cycle slips estimated value; (b) PRN40 cycle slips estimated value.

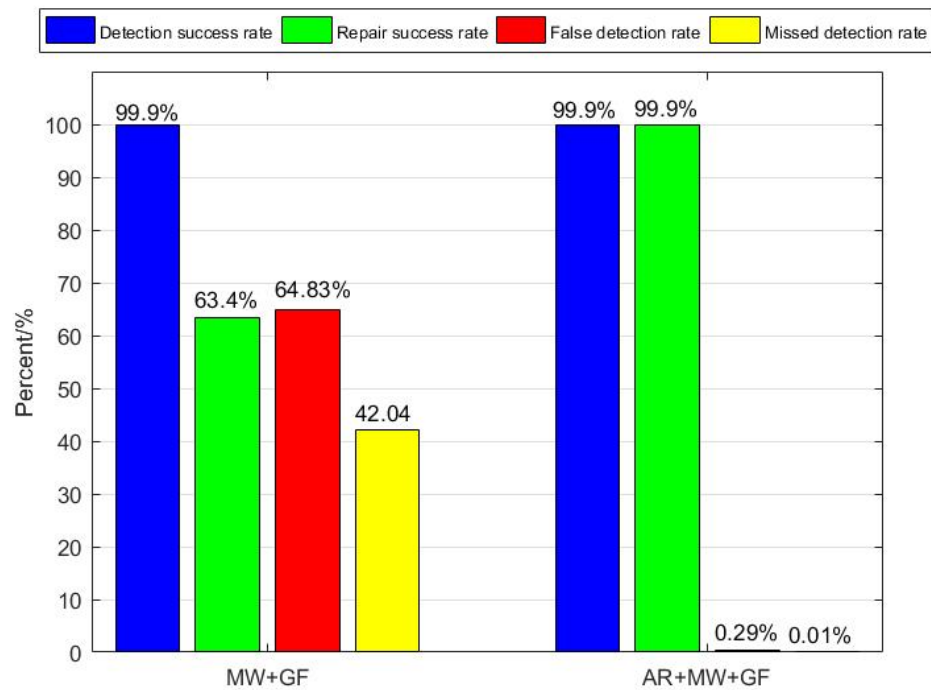


Figure 12. Comparison of cycle slips completeness detection in multipath environment.

Table 3. Cycle slips repair results.

PRN	Position	Cycle Slips	(Traditional Methods) Calculated Value of Cycle Slips/Cycle	Cycle Slips Repair Value/Cycle	(AR Assisted Model) Calculated Value of Cycle Slips/Cycle	Cycle Slips Repair Value/Cycle
C38	200	(1, 1)	(0.789, 2.238)	(1, 2)	(0.947, 1.061)	(1, 1)
C38	400	(2, 4)	(3.114, 3.076)	(3, 3)	(2.010, 4.018)	(2, 4)
C38	800	(8, 6)	(9.482, 4.879)	(9, 5)	(7.905, 6.018)	(8, 6)
C38	1200	(1, -2)	(-0.788, -1.825)	(-1, -2)	(1.053, -2.026)	(1, -2)
C38	1500	(-1, 1)	(0.747, 2.945)	(1, -3)	(-1.095, 0.939)	(-1, 1)
C38	1800	(5, 3)	(3.959, 3.489)	(4, 3)	(4.958, 3.057)	(5, 3)
C40	200	(1, 1)	(3.245, 0.868)	(3, 1)	(1.037, 1.065)	(1, 1)
C40	400	(2, 4)	(2.736, 3.568)	(3, 4)	(1.895, 3.961)	(2, 4)
C40	800	(8, 6)	(6.255, 7.120)	(6, 7)	(8.042, 5.982)	(8, 6)
C40	1200	(1, -2)	(1.047, 1.822)	(1, 2)	(0.8897, -2.018)	(1, -2)
C40	1500	(-1, 1)	(0.257, 3.119)	(0, 3)	(-1.005, 0.921)	(-1, 1)
C40	1800	(5, 3)	(5.473, 2.333)	(5, 2)	(4.947, 3.000)	(5, 3)

As shown in Figure 11, the results indicate that, on the one hand, for the carrier phase observations at B1c and B2a with the same period of small cycle slips (e.g., at 700 epochs), the MW combination does not detect the cycle slips successfully, but the GF method clearly detects them, because the MW combination cannot detect the same cycle slips at the same epoch for both frequencies. On the other hand, for the cycle slips (8,6) of the frequencies B1c and B2a at 1300 epoch, the GF combination cannot detect accurately, because the cycle slips' ratio in the carrier phase observation values of the B1C and B2A frequencies is very close to the ratio of the two frequencies. In a weak multipath environment, the GF + MW model can detect most types of cycle slips, but in a severe multipath environment, if there are special cycle scale situations (such as: 1300 epoch), the GF combination is unable to detect cycle slips due to the existence of some kind of detection blind spots. Furthermore, the MW combination can detect if cycle slips occurred, but the result is not accurate. This is because the multipath effect seriously affects the pseudorange accuracy and leads to the failure of the MW + GF model. At this time, the MW + GF combination fails in the severe multipath environment. In contrast, the AMG combination is not affected by the pseudorange multipath, and cycle slips can still be accurately detected and successfully

repaired in severe multipath environments. As shown in Figure 12, the cycle slips' repair success rate of the MW + GF detection model in the multipath environment is 63.4%, because when the pseudo range multipath effect is serious, the false detection rate rises linearly, and it is easy to mistakenly detect the pseudo range multipath effect as the cycle slips. Especially for the combined wavelengths of the dual-frequency signals, the false detection is more serious. For the simulated large and small cycle slips, the AMG combined detection model can detect them effectively.

Compared with the traditional TurboEdit methods, the AMG method can effectively detect cycle slips under severe multipath conditions, whose cycle slips' estimation is not affected by the multipath residual, and the success rate of the cycle slips' recovery is even higher. As shown in Table 3, due to the serious influence of the multipath effect on the accuracy of the pseudorange, the cycle slips' repair with the traditional method failed (such as: 700, 900, 1300 epoch, etc.). The results show that the accuracy of the pseudorange seriously affects the success rate of the cycle slips' repair. When the AMG method was used to repair the cycle slips, we used AR to predict and restore the pseudorange in the severe multipath environment, which improved the success rate of the cycle slips' repair (such as: 700, 900, 1300, epoch, etc.), and the success rate of the rounded repair reached 99.9%.

4. Conclusions

Geographic information services and geoprocessing services require BDS high-precision positioning technology to provide accurate spatial and temporal services. However, in severe urban environments, frequent shading will lead to multipathing, which will cause cycle slips of BDS observations, and the positioning accuracy is affected by these frequent cycle slips. To enhance the capability of the geoprocessing services and solve the problem of the cycle slips' detection and repair of the BDS-3 dual-frequency observation in severe multipath environments, an AMG method for the detection of cycle slips is proposed in this paper. Firstly, pseudorange observations unaffected by the multipath are used as the training quantity; an AR model based on the sliding-window method is constructed to predict the reliable pseudorange observations in a severe multipath environment. Then, the cycle slips' detection was carried out combining AR with the MW + GF method, and a derivation model and completeness monitoring indicators are derived to verify the effectiveness of the algorithm in theory. The field test results show that when the MW + GF combination fails in the severe multipath environments, the AMG combination still maintains a powerful detection and repair ability. Compared with the MW + GF method, the cycle slips' repair success rate of the AMG method is increased by 36%, and the cycle slips false detection rate and the missed detection rate are reduced by 64.5% and 42.0%, respectively. The specific contribution of this paper is:

- (1) Compared with the traditional MW + GF method, the advantages of our method are: (1) the influence of the multipath effect on the MW observation equation has been significantly weakened, the probability of the false detection and missing detection of the cycle slips has been dramatically reduced, the more accurate estimation of the cycle slips has been obtained, and the success rate of the cycle slips' detection is more accurate. (2) The AMG method effectively solves the failure of the cycle slips' collection and repair in severe multipath conditions and restores the pseudorange in the multipath environment through an AR prediction. The cycle slips' estimation is not affected by the residual of the pseudorange multipath, and the success rate of the cycle slips' collection and repair is higher.
- (2) For the simulated cycle slips in the B1c and B2a dual-frequency observations of two types of BDS-3 satellites, the results show that the conventional MW + GF combination fails. After adopting the method in this paper, the detection and repair ability of the cycle slips has been significantly improved and reached the practical level. The false detection rate is 0.29%, the missed detection rate is 0.01%, the detection success rate is 99.9%, and the repair success rate is 99.9%.

- (3) The AMG method proposed in this paper has been verified experimentally in the severe multipath environment. However, the AMG method proposed in this paper needs to be trained with clean pseudorange data in advance, which has limitations in the practical real-time application of the cycle slips' detection and repair. In the future, we will consider this shortcoming and constantly improve the practicability of the AMG method. What calls for special attention is that the values presented in the conclusion were obtained for the field data conditions analyzed in this paper. The multipath can vary greatly according to the environment and these values of the PF and PA will not remain constant depending on their test environment.

Author Contributions: Conceptualization, Y.N. and J.C.; methodology, D.C.; software, W.Z.; validation, J.C. and D.C.; formal analysis, W.Z.; investigation, Y.N.; resources, W.Z.; data curation, J.C.; writing—original draft preparation, J.C.; writing—review and editing, J.C.; visualization, Y.N. and Y.S.; supervision, J.X. and S.W.; project administration, J.X. and S.W.; funding acquisition, Y.S. All authors have read and agreed to the published version of the manuscript.

Funding: This research was supported by Natural Science Foundation of China (grant numbers 42204011) and partly supported by the Natural Science Foundation of Shandong Province (grant numbers ZR2022QD108; grant numbers ZR2021QD058).

Institutional Review Board Statement: The study did not require ethical approval.

Informed Consent Statement: Not applicable.

Data Availability Statement: Not applicable.

Conflicts of Interest: The authors declare no conflict of interest.

References

1. Xing, H.; Chen, J.; Wu, H.; Zhang, J.; Li, S.; Liu, B. A service relation model for web-based land cover change detection. *Int. J. Photogramm. Remote Sens.* **2017**, *132*, 20–32. [CrossRef]
2. Xing, H.; Hou, D.; Wang, S.; Yu, M.; Meng, F. O-LCMapping: A Google Earth Engine-based web toolkit for supporting online land cover classification. *Earth Sci. Inform.* **2021**, *14*, 529–541. [CrossRef]
3. Zhu, L.; Xing, H.; Hou, D. Analysis of carbon emissions from land cover change during 2000 to 2020 in Shandong Province, China. *Sci. Rep.* **2022**, *12*, 8021. [CrossRef] [PubMed]
4. Xing, H.; Zhu, L.; Feng, Y.; Wang, W.; Hou, D.; Meng, F.; Ni, Y. An Adaptive Change Threshold Selection Method Based on Land Cover Posterior Probability and Spatial Neighborhood Information (Odolinski and Teunissen, 2018). *IEEE J. Sel. Top. Appl. Earth Obs. Remote Sens.* **2021**, *14*, 11608–11621. [CrossRef]
5. Yang, Y.; Gao, W.; Guo, S.; Mao, Y.; Yang, Y. Introduction to BeiDou-3 navigation satellite system. *Navigation* **2019**, *66*, 7–18. [CrossRef]
6. Yang, Y.; Liu, L.; Li, J.; Yang, Y.; Zhang, T.; Mao, Y.; Sun, B.; Ren, X. Featured services and performance of BDS-3. *Sci. Bull.* **2021**, *66*, 2135–2143. [CrossRef]
7. Bei Dou Navigation Satellite System Signal in Space Interface Control Document Open Service Signal B2a (Version 1.0). Available online: <http://www.beidou.gov.cn/yw/xwzx/201712/W020171226734109297599.pdf> (accessed on 27 December 2017).
8. Yang, Y.; Long, J.; Xu, J.; Tang, J.; He, H. Contribution of the Compass satellite navigation system to global PNT users. *Chin. Sci. Bull.* **2011**, *56*, 2813–2819. [CrossRef]
9. Wang, H.; Pan, S.; Gao, W.; Ye, F.; Ma, C.; Tao, J.; Wang, Y. Real-Time Cycle Slip Detection and Repair For BDS-3 Triple-frequency and Quad-Frequency B1C/B1I/B3I/B2A Signals. *Acta Geodyn. Geomater.* **2021**, *18*, 363–377. [CrossRef]
10. Li, Z.; Huang, J. *GPS Surveying and Data Processing*, 3rd ed.; Wuhan University Press: Wuhan, China, 2016; pp. 156–158.
11. Zhao, J.; Hernández-Pajares, M.; Li, Z.; Wang, L.; Yuan, H. High-rate Doppler-aided cycle slip detection and repair method for low-cost single-frequency receivers. *GPS Solut.* **2020**, *24*, 80. [CrossRef]
12. Li, D.; Dang, Y.; Yuan, Y.; Mi, J. A New Cycle-Slip Repair Method for Dual-Frequency BDS Against the Disturbances of Severe Ionospheric Variations and Pseudoranges with Large Errors. *Remote Sens.* **2021**, *13*, 1037. [CrossRef]
13. Banville, S.; Langley, R. Mitigating the impact of ionospheric cycle slips in GNSS observations. *J. Geod.* **2013**, *87*, 179–193. [CrossRef]
14. Ke, J.; Lu, X.; Wang, X.; Chen, X.; Tang, S. Decoding Performance Analysis of GNSS Messages with Land Mobile Satellite Channel in Urban Environment. *Electronics* **2018**, *7*, 273. [CrossRef]
15. Yu, S.; Liu, Z. The ionospheric condition and GPS positioning performance during the 2013 tropical cyclone usagi event in the Hong Kong region. *Earth Planets Space* **2021**, *73*, 66. [CrossRef]
16. Blewitt, G. An automatic editing algorithm for GPS data. *Geophys. Res. Lett.* **1990**, *17*, 199–202. [CrossRef]

17. Lima, F.; Moraes, A. Modeling multifrequency GPS multipath fading in land vehicle environments. *GPS Solut.* **2021**, *25*, 1–14.
18. Miao, Y.; Sun, Z.; Wu, S. Error Analysis and Cycle-Slip Detection Research on Satellite-Borne GPS Observation. *J. Aerosp. Eng.* **2011**, *24*, 95–101. [[CrossRef](#)]
19. Xu, X.; Nie, Z.; Wang, Z.; Zhang, Y. A Modified TurboEdit Cycle-Slip Detection and Correction Method for Dual-Frequency Smartphone GNSS Observation. *Sensors* **2020**, *20*, 5756. [[CrossRef](#)]
20. Dong, Y.; Dai, P.; Wang, S.; Xing, J.; Xue, Y.; Liu, S.; Han, S.; Yang, Z.; Bai, X. A Study on the Detecting Cycle Slips and a Repair Algorithm for B1/B3. *Electronics* **2021**, *10*, 2925. [[CrossRef](#)]
21. Cai, C.; Liu, Z.; Xia, P.; Dai, W. Cycle slip detection and repair for undifferenced GPS observations under high ionospheric activity. *GPS Solut.* **2013**, *17*, 247–260. [[CrossRef](#)]
22. Shi, Z.; Dong, X.; Qian, Z.; Sun, X.; Hu, Y. A new real-time cycle slip detection and repair approach based on BDS dual-frequency carrier phase and Doppler observations. *IET Radar Sonar Navig.* **2022**, *16*, 51–63. [[CrossRef](#)]
23. Li, F.; Gao, J.; Li, Z.; Qian, N. A step cycle slip detection and repair method based on double-constraint of ephemeris and smoothed pseudorange. *Acta Geodyn. Geomater.* **2019**, *16*, 337–348. [[CrossRef](#)]
24. Gao, W.; Meng, X.; Gao, C.; Pan, S.; Zhu, Z.; Xia, Y. Analysis of the carrier-phase multipath in GNSS triple-frequency observation combinations. *Adv. Space Res.* **2018**, *63*, 2735–2744. [[CrossRef](#)]
25. Ning, Y.; Wang, J.; Hu, X.; Wang, S. Inertial Aided Cycle-slip Detection and Repair for BDS Triple-frequency Signal in Severe Multipath Environment. *Acta Geod. Cartogr. Sinaica* **2016**, *45*, 179–187.
26. Kim, J.; Park, M.; Bae, Y.; Kim, O.; Kee, C. A Low-Cost, High-Precision Vehicle Navigation System for Deep Urban Multipath Environment Using TDCP Measurements. *Sensors* **2020**, *20*, 3254. [[CrossRef](#)]
27. Qian, N.; Gao, J.; Li, Z.; Fang, C.; Pan, C. GPS/BDS triple-frequency cycle slip detection and repair algorithm based on adaptive detection threshold and FNN-derived ionospheric delay compensation. *Acta Geodyn. Geomater.* **2020**, *17*, 141–156. [[CrossRef](#)]
28. Wang, J.; Hu, X.; Ning, Y.; Yao, Y. Cycle-slip detection and correction for BDS triple-frequency observations under strong ionospheric conditions. *J. Chin. Inert. Technol.* **2017**, *25*, 71–76.
29. Gan, Y.; Sui, L.; Guo, B.; Wen, J. Improving the performance of mw combined observation on cycle slip detection using emd threshold de-noising. *J. Geomat. Sci. Technol.* **2015**, *35*, 666–670.
30. Shi, J.; Gao, Y. A comparison of three PPP integer ambiguity resolution methods. *GPS Solut.* **2014**, *18*, 519–528. [[CrossRef](#)]
31. Liu, T.; Chen, Q.; Geng, T.; Jiang, W.; Chen, H.; Zhang, W. The benefit of Galileo E6 signals and their application in the real-time instantaneous decimeter-level precise point positioning with ambiguity resolution. *Adv. Space Res.* **2022**, *69*, 3319–3332. [[CrossRef](#)]
32. Chai, D. Study on the Theory and Method in Integrated Navigation of Multi-constellation GNSS/INS. Ph.D. Thesis, China University of Mining and Technology, Xuzhou, China, 2020.
33. Pan, Z.; Cheng, X.; Cheng, S.; Wang, T.; Zhai, Y.; Zou, J.; Wang, C. *Digital Topographic Survey*, 2nd ed.; Wuhan University Press: Wuhan, China, 2015; pp. 55–59.
34. Altmayer, C. Enhancing the integrity of integrated GPS/INS systems by cycle slip detection and correction. In Proceedings of the IEEE Intelligent Vehicles Symposium 2000, Dearborn, MI, USA, 6 August 2002.
35. Han, H.; Wang, J.; Li, Z.; Wang, Y. Inertial Aided Kinematic GPS Cycle Slip Detection and Correction for GPS/INS Tightly Coupled System. *Acta Geod. Cartogr. Sinaica* **2015**, *44*, 848–857.
36. Ge, M.; Gendt, G.; Rothacher, M.; Shi, C.; Liu, J. Resolution of GPS Carrier-Phase Ambiguities in Precise Point Positioning (PPP) with Daily Observations. *J. Geod.* **2008**, *82*, 389–399. [[CrossRef](#)]
37. Dong, D.; Bock, Y. Global Positioning System Network Analysis with Phase Ambiguity Resolution Applied to Crustal Deformation Studies in California. *J. Geophys. Res. Solid Earth (1978–2012)* **1989**, *94*, 3949–3966. [[CrossRef](#)]
38. Cheng, P.; Li, W.; Bei, J. Precision Analysis of BeiDou Range Measurement Signal. *Acta Geod. Cartogr. Sin.* **2012**, *41*, 690–695+708.

Disclaimer/Publisher’s Note: The statements, opinions and data contained in all publications are solely those of the individual author(s) and contributor(s) and not of MDPI and/or the editor(s). MDPI and/or the editor(s) disclaim responsibility for any injury to people or property resulting from any ideas, methods, instructions or products referred to in the content.